Journal of Power Sources 201 (2012) 184–195

Contents lists available at SciVerse ScienceDirect

Journal of Power Sources

journal homepage: www.elsevier.com/locate/jpowsour

A PDE model for microscopic simulation of solid oxide fuel cells

Mario Angeloni*, Pilar Lisbona, Roberto Bove

Industrial Engineering Department, University of Perugia, Via G. Duranti 67, 06125 Perugia, Italy

ARTICLE INFO

Article history:
Received 11 July 2011
Received in revised form 26 October 2011
Accepted 31 October 2011
Available online 6 November 2011

Keywords:
Solid oxide fuel cell
Modelling
Planar
Anode supported

ABSTRACT

A mathematical model of a single unit solid oxide fuel cell (SOFC) based on partial differential equations is presented in this paper. The model consists of mass, momentum and charge conservation equations, relating gas concentration to voltage, current density, and other relevant fuel cell parameters. The model is applied and validated on a planar disk-shape anode-supported cell. Data regarding materials' properties and kinetic parameters are taken from the open literature or derived from experimental results. A commercial tool using the finite element method is used to solve the set of equations. The simulated steady state performance of the fuel cell, for different operating conditions and current densities, is further investigated.

1. Introduction

The structure of a mathematical model for fuel cells (FC) simulation usually depends on the purpose of the model itself. When, for example, the main purpose of the model is to provide FC performance, in order to analyze the whole system (or power plant) performance, the variation of physical–chemical variables (such as gas concentration, temperature, pressure and current density, for example) are not relevant; however the performance, in terms of power, heat and input requirements are important. On the other hand, if the focus of the investigation is the design of a stack, a single cell, or even a specific component of the cell, a model that considers a detailed description of each phenomenon taking place within the fuel cell is needed.

According to the level of details considered, mathematical models for fuel cells may be classified as:

- Black-box models [1], where single cells or stacks are represented as non-dimensional devices with a number of mass and energy inputs and outputs. Transport phenomena occurring within the system are not simulated with this approach, but mass and energy balances are solved for computing the inlet and outlet streams' properties, as well as for estimating fuel cell power and efficiency. These models are not suitable to analyze phenomena occurring within a fuel cell, but they are a necessary tool for analyzing how the fuel cell affects other parts of the system [2,3].
- Single cell models with details of the cell components [4–10]. These models describe the behaviour of concentration of chemical species, gas velocity, temperature, current and the distribution of other physical parameters in the fuel cell, and they are usually used as design tools to optimize geometry parameters and dimensions of the single cell or of the stack (e.g. electrodes thickness, rib width) and to predict the operating conditions.
- The last approach is the microscopic one, in which diffusion and adsorption phenomena are studied in detail and parameters used in the macroscopic models, such as porosity, tortuosity, and activation energy can be estimated.

The last two model approaches are more complex than the first one, and numerical methods must be used for solving the systems of partial differential equations.

Mathematical models describing electrochemical and/or fluid dynamic performance of the fuel cell may be: one-dimensional when parameters are considered to vary only in one direction (usually the flow direction) [9], two-dimensional when phenomena are modelled to vary over a cross-section as representative behaviour of the entire cell performance [4,5] and three-dimensional when phenomena are considered to vary within the whole domain and parameter variations in every direction are taken into account. Simplifications and assumptions which lead to 1D and 2D models must be carefully chosen to minimize the distortion of reality that they introduce and to avoid neglecting of those phenomena which are relevant for the possible application of the model.

Most mathematical models available in the open literature do not consider the evolution of all the parameters within all the dimensions of the domain considered. Even for 3D models, the most frequent approach is to assume a lumped Positive

* Corresponding author. Tel.: +34 976506520; fax: +34 976506644.
E-mail addresses: mario@litec.csic.es, angeloni.mario@gmail.com (M. Angeloni).

0378-7753/$ – see front matter © 2011 Elsevier B.V. All rights reserved.
doi:10.1016/j.jpowsour.2011.10.109

Nomenclature

D_{ij}	diffusion coefficient in a binary system [$m^2\ s^{-1}$]
$D_{i,K}$	Knudsen diffusion coefficient [$m^2\ s^{-1}$]
$D_{i,eff}$	effective diffusion coefficient [$m^2\ s^{-1}$]
e	percentual error [–]
E_{act}	activation energy [$J\ mol^{-1}$]
E_0	ideal Nernst voltage at standard pressure [V]
F	Faraday constant [$C\ mol^{-1}$]
$\vec{J}$	current density [$A\ m^{-2}$]
J_0	exchange current density [$A\ m^{-2}$]
$h_{channel}$	height of the gas channel [m]
M_i	molecular weight of component i [$g\ mol^{-1}$]
M	molecular weight of gas mixture [$g\ mol^{-1}$]
N_i	mass flow of component i [$kg\ m^{-2}\ s^{-1}$]
n	number of electrons involved in the electrochemical reaction [–]
OCV	open circuit voltage [V]
P	pressure [Pa]
P_{ref}	reference pressure [Pa]
P_i	partial pressure of component i [Pa]
P_i'	partial pressure of component i at the electrode/electrolyte interface [Pa]
$Q_{an,cat}$	volumetric anode or cathode flow rate [$kg\ s^{-1}$]
r_{manif}	radius of the cell section where the flow configuration changes from normal to radial [m]
R_g	universal gas constant [$J\ mol^{-1}\ K^{-1}$]
T	cell temperature [K]
T_0	standard temperature [K]
$\vec{u}$	gas velocity [$m\ s^{-1}$]
$U_{an,cat}$	gas inlet velocity [$m\ s^{-1}$]
U_f	coefficient of utilization [–]
V_{rev}	reversible voltage [V]
V_{cell}	cell voltage [V]
Y_i	mass fraction of component i [–]

Subscripts

act	activation
an	anode side
cat	cathode side
conc	concentration
el	electric
ion	ionic

Superscripts

lab	laboratory
sim	simulation

Greek letters

α_{OCV}	corrective coefficient [–]
β	symmetry factor of Butler–Volmer equation [–]
ε	porosity [–]
ϕ	potential [V]
γ	pre-exponential factor [$A\ m^{-2}$]
μ	dynamic viscosity [$kg\ m^{-1}\ s^{-1}$]
η	voltage loss [V]
ρ	density [$kg\ m^{-3}$]
ρ_{el}	electronic density [$C\ m^{-3}$]
ρ_{ion}	ionic density [$C\ m^{-3}$]
σ	electric/ionic conductivity [$S\ m^{-1}$]
τ	tortuosity [–]

Electrode-Electrolyte-Negative Electrode (PEN) structure for modelling the current density and electrical potential distribution in the direction perpendicular to the flow direction [4–9].

The result of such assumption is a fast converging solution. On the other hand, information on current density, electrical potential distribution and gas species concentrations within the PEN domain is neglected. Furthermore, such models are restricted to a specific geometry. They cannot simulate other fuel cells with slight geometry variations. Bjaradwaj et al. [4,5], for example, developed two different models for simulating the operation of two SOFCs, one tubular and the other flat tubular (both SOFC types are produced by Siemens Westinghouse Power Corporation).

The time consuming process of defining a new model for every geometry modification is not present if all the equations are in a partial differential form (PDE) [11–16]. This feature is of particular importance during the design and improvement phase of a SOFC, when different geometrical configurations need to be compared.

Bove and Ubertini [16] show how most models found in the literature can be considered simplifications of a mathematical model, entirely based on partial differential equations, where the variation of all the involved variables is considered in the entire domain. Limitations and simplifications introduced with each modelling approach are also highlighted.

In the present study, the mathematical model described in [16] is applied and validated on a planar disk-shape anode-supported cell. The same model was previously applied for a micro-tubular SOFC geometry, without significant modifications [15]. The results allowed one to evaluate different performance of a micro-tubular SOFC, relative to different current collector configurations.

In the present study, the model is presented in a 3D, time-dependent form, and is implemented for a 2D geometry, under steady-state conditions.

2. Fuel cell geometry

The model is applied to a planar disk-shape SOFC shown in Fig. 1 currently produced by InDEC B.V, and operated at the Fuel Cell Lab of the University of Perugia.

The anode material is a cermet nickel oxide doped with yttrium stabilized zirconia, 8% yttrium (NiO/8YSZ). The cathode is made of 8YSZ with strontium-doped $LaMnO_3$ (8YSZ/LSM), and the electrolyte consists of dense 8YSZ.

As shown in Fig. 1, the anodic and cathodic flows are introduced perpendicularly to the plane of the cell, on the two opposite sides, through two alumina tubes (not represented in Fig. 1). The anodic and cathodic flows have a mirror symmetric configuration, thus hereinafter in this section, the description of the anodic or cathodic flow is simply referred to as “flow”, indifferently if referred to the anode or to the cathode.

The flow reaches the electrode surface in a circular region, where it changes its direction from perpendicular to radial, with respect to the fuel cell plane, and proceeds along the electrode surface in a co-flow configuration. The electrical current is drawn from the cell through a mesh (Pt for the cathode and Ni for the anode), located between the cell housing and the electrode. In the present study, the effect of such mesh on the velocity field of the gas in the gas channel is neglected, due to the laminar regime within the whole cell. Fig. 2 shows the Reynolds number in both gas channels for $V = 0.656$ V. The effect of the different gas flows in the channels on Reynolds number values is clearly observed since cathodic gas flow exceed five times the anodic one.

The geometrical dimensions of the single cell are presented in Table 1.

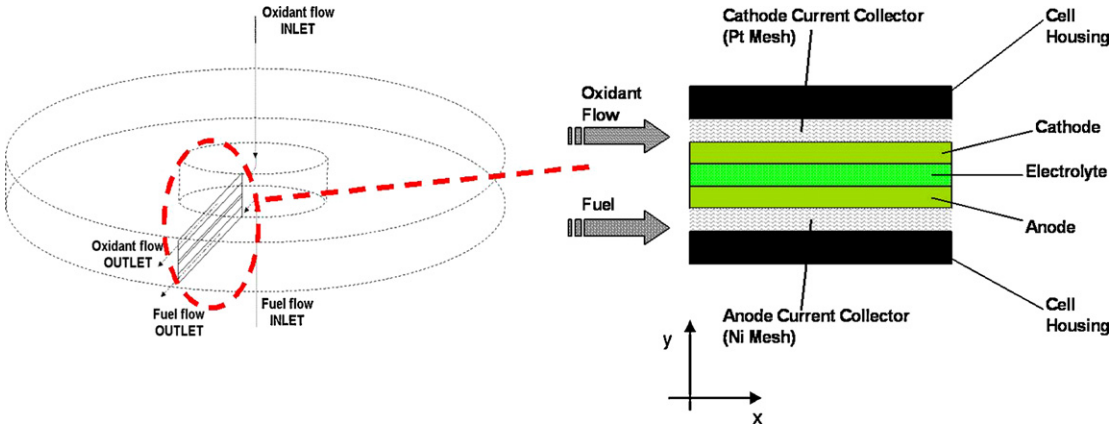

Fig. 1. Planar disk-shape SOFC considered in the present study.

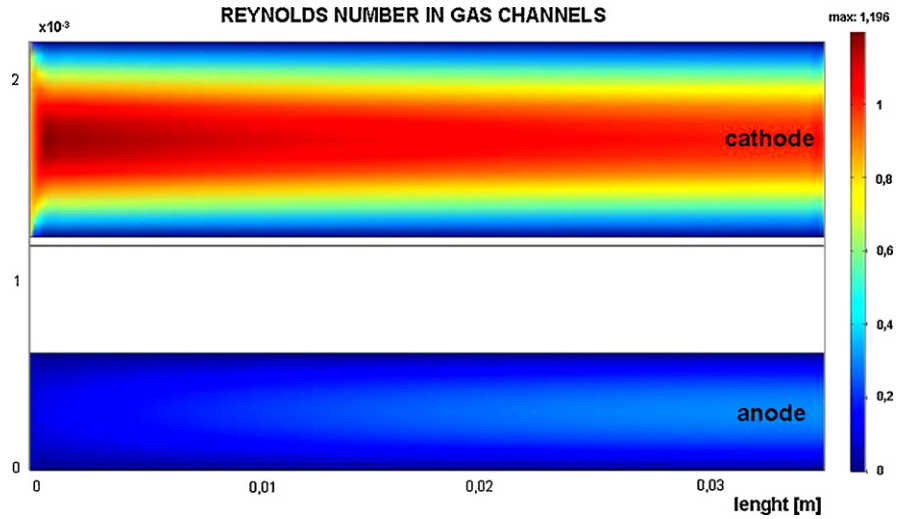

Fig. 2. Reynolds number in gas channels for $V = 0.656$ V.

3. Process description

As shown in Fig. 1, once the gas starts flowing radially, it is in contact with, and permeates, the porous electrode (anode or cathode). Diffusion takes place in the whole electrode domain, and proceeds towards the reaction zone which is very close to the electrode/electrolyte interface. Since both electrodes are electrically conductive, electrons coming from (going to) an external circuit flow through it. Oxygen provided at the cathode side, once having reached the reaction zone, combines with electrons to produce oxygen ions, according to the following reaction:

$$\frac{1}{2}O_2 + 2e^- \rightarrow O^{2-} \quad (1)$$

The electrolyte presents high electrical resistance and high ionic conductivity, thus, ideally, only ions flow through it. Moreover the dense structure does not allow any molecular permeation. At the anode side, ions coming from the electrolyte react with hydrogen:

$$H_2 + O^{2-} \rightarrow H_2O + 2e^- \quad (2)$$

Reactions (1) and (2) take place where there is a simultaneous presence of electrons, ions and gases, i.e. in the so-called triple-phase-boundary (TPB). As a consequence of the reactions, water, electricity and heat are produced. Water generated in the anode side diffuses to reach the gas channel and leaves the cell. Electrons released in reaction (2), migrating through the anode, are collected through the current collector, and are transferred to the cathode through an external load. At the cathode side, these electrons flow from the current collector to the cathodic reaction zone. In this way, a close external electrical circuit is created.

Table 1
Tested planar disk-shape dimensions.

Active area	4848 mm^2
Anode thickness	545 μm
Cathode thickness	40 μm
Electrolyte thickness	5 μm
Cathode channel height	1 mm
Anode channel height	0.6 mm
Channels width	1.51 mm

4. Mathematical model

A complete mathematical model must consider all the transport phenomena occurring within the fuel cell, as described in Section 3. Heat transport, charge transport, mass diffusion and convection take place simultaneously in several domains of the fuel cell.

In the present study, each sub-domain (i.e. anode, cathode, and electrolyte) is modelled independently from the other following the model proposed by Bove and Ubertini [16], and no lumped structures are considered. Phenomena occurring in different

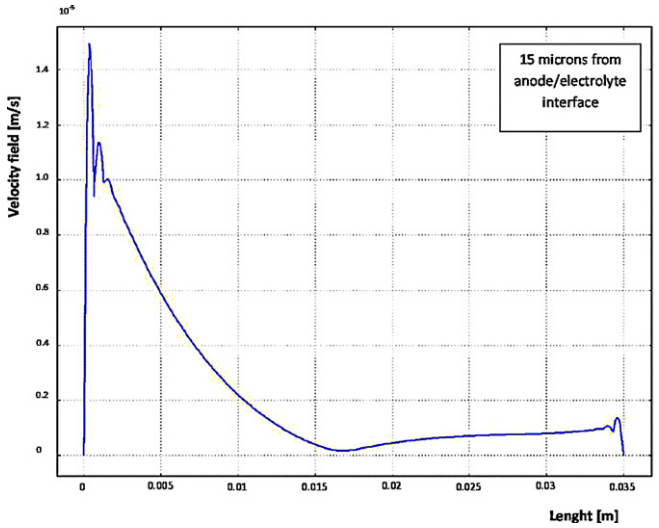

Fig. 3. Velocity field in a longitudinal section of the anode (15 μm from anode/electrolyte interface).

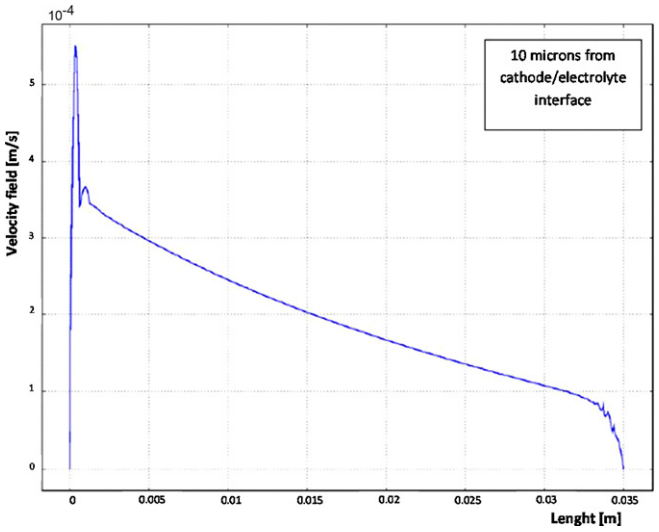

Fig. 4. Velocity field in a longitudinal section of the cathode (10 μm from cathode/electrolyte interface).

sub-domains are linked to each other by appropriate boundary or interface conditions.

Energy balance is not included because the SOFC used in the experiments was operated at constant temperature, guaranteed by an electric oven. The validation of the energy balance would thus be extremely hard to obtain, and, more importantly, the isothermal conditions would not reflect the real operation of a single cell of a stack. It must be noted, in fact, that temperature distribution is very non-uniform within a single cell embedded in a stack [17], while in the present situation, the cell is mostly at isothermal condition.

Some assumptions have been made to simplify conservation and constitutive laws:

(1) Electrochemical reactions are confined at the electrode/electrolyte interface.
(2) Constant temperature within the cell
(3) Constitutive law for ideal gas

Additional assumptions are introduced for each single subdomain, and, for sake of clarity, they are presented in the specific sections.

4.1. Conservation and constitutive equations

Mass, chemical species, momentum and charge conservation laws are applied in the different domains. Mass, species and momentum conservation equations are considered in the gas channels. The charge conservation is applied in the anode, the cathode and the electrolyte.

In the porous media, mass transport is assumed to occur mainly by diffusion, therefore, momentum balance coupled with the *constitutive law* for porous media (e.g. Darcy's law or Brinkman's equation) is neglected. This assumption has been verified by preliminary simulations, where Brinkman's equation is implemented and a negligible effect is demonstrated. Figs. 3 and 4 present the profiles of convective velocity field in a section of anode and cathode respectively, when Brinkman's equation is implemented. As can be noted, anode and cathode convective velocity are almost zero (order of magnitude 10^{-5} m s^{-1}), thus convective flows (order of magnitude 10^{-7} to 10^{-6} mol m^{-2} s^{-1}) in the electrodes are negligible compared to diffusive flows (order of magnitude 10^{-2} to 10^{-1} mol m^{-2} s^{-1}). The diffusion of chemical species is modelled by Fick's law. Convection and diffusion phenomena have been considered to model the balance of chemical species in the gas channels.

The charge conservation equation is applied to electrode (electric charge) and electrolyte domain (ionic charge). The *constitutive law* to describe these charge transport phenomena is Ohm's law.

4.2. Gas channels

According to the conservative and consecutive equations referred in Section 4.1, the set of equations describing fluid behaviour in gas channels is:

$$\frac{\partial \rho}{\partial t} + \nabla(\rho \vec{u}) = 0 \tag{3}$$

$$\frac{\partial \rho Y_i}{\partial t} + \vec{u}\vec{\nabla}(\rho Y_i) = \nabla(\rho D_{ij}\vec{\nabla} Y_i) \tag{4}$$

$$\rho\frac{\partial \vec{u}}{\partial t} + \rho(\vec{u}\nabla\vec{u}) = -\vec{\nabla}P + \mu\nabla^2\vec{u} \tag{5}$$

Eq. (4) is obtained from the conservation law of chemical species and Fick's law, considering that no reactions take place in the gas channels (assumption 1). Eq. (4) becomes four equations when applied to the chemical species in gas channel streams: H_2 and H_2O in the anode side, O_2 sand N_2 in the cathode side. In obtaining Eq. (5), body forces within the gas channels have been neglected. The assumption of ideal gas introduces the expression of density, which completes the system of equations:

$$P = \frac{\rho}{M}R_g T \tag{6}$$

The dynamic viscosity of a gas mixture has been calculated with Herning and Zipperer formula, proposed by Shan et al. [18]. For the single chemical species of the mixture, dynamic viscosity has been taken from an empirical correlation proposed by Todd and Young [19]. Fuller-Schettler-Gidding correlation [20] has been used to calculate the diffusion coefficient D_{ij} of a binary mixture.

4.3. Electrodes

In this case, the porous nature of the electrodes is taken into account in defining the binary diffusion coefficients. The following expressions are derived, respectively, for anode and cathode:

$$\frac{\partial \rho Y_i}{\partial t} = \nabla(\rho D_{O_2-N_2,\text{porous}}\vec{\nabla} Y_i) \tag{7}$$

Fig. 5. Detail of the single fuel cell test rig in the fuel cell laboratory at the University of Perugia.

$$\frac{\partial \rho Y_i}{\partial t} = \nabla(\rho D_{H_2O-H_2,\text{porous}} \vec{\nabla} Y_i) \tag{8}$$

If the Knudsen number, $Kn = \lambda/D_{\text{pore}}$, is near 1 or higher than 1, Knudsen diffusion is important. λ in Knudsen number expression represents the mean free path of the gas. As stated in [20,21], Knudsen diffusion should be considered when dealing with SOFC porous electrodes mass transport. The diffusion coefficients in the porous media take into account Knudsen diffusion coefficient $D_{i,K}$ which considers the interaction between molecules and pore walls and the binary diffusion coefficient.

$$D_{O_2,\text{eff}} = \left(\frac{1}{D_{ij,\text{porous}}} + \frac{1}{D_{O_2,K}}\right)^{-1} \tag{9a}$$

$$D_{N_2,\text{eff}} = \left(\frac{1}{D_{ij,\text{porous}}} + \frac{1}{D_{N_2,K}}\right)^{-1} \tag{9b}$$

$$D_{H_2,\text{eff}} = \left(\frac{1}{D_{ij,\text{porous}}} + \frac{1}{D_{H_2,K}}\right)^{-1} \tag{10a}$$

$$D_{H_2O,\text{eff}} = \left(\frac{1}{D_{ij,\text{porous}}} + \frac{1}{D_{H_2O,K}}\right)^{-1} \tag{10b}$$

The effective diffusion coefficients of a binary mixture in a porous medium are calculated through the following expression, taken from Aguiar et al. [22]:

$$D_{ij,\text{porous}} = D_{ij}\frac{\varepsilon}{\tau} \tag{11}$$

Besides the mass transport, the electric problem is described within the electrodes domain. The charge conservation equation, coupled with Ohm's law yields:

$$\frac{\partial \rho_{\text{el}}}{\partial t} + \nabla(\sigma_{\text{el}} \vec{\nabla}\phi) = 0 \tag{12}$$

Additionally, charge conservation equation is solved to determine the current density distribution within the electrodes domain.

4.4. Electrolyte

The only phenomenon considered in this domain is the ion transportation, O^{2-}, from cathode to anode interface.

$$\frac{\partial \rho_{\text{ion}}}{\partial t} + \nabla(\sigma \vec{\nabla}\phi_{\text{ion}}) = 0 \tag{13}$$

Table 2
Model parameters and material properties.

Parameter	Units	Calibrated value	Literature
$E_{a,an}$	[J mol^{-1}]	128,000	100,000[8]
$E_{a,cat}$	[J mol^{-1}]	122,000	120,000[8]
γ_{an}	[A m^{-2}]	1×10^9	5.5×10^8[8]
γ_{cat}	[A m^{-2}]	1×10^9	7×10^8[8]
σ_{ion}	[Ω^{-1} m^{-1}]	2.26383	2.26383[9]
σ_{an}	[Ω^{-1} m^{-1}]	30315.4	30315.4[9]
σ_{cat}	[Ω^{-1} m^{-1}]	12792.4	12792.4[9]
ε	[–]	0.3	0.3[18]
τ	[–]	10	6[18]
D_{N_2}	[m^2 s^{-1}]	5.692×10^{-6}	8.322×10^{-6}[18,21]
D_{O_2}	[m^2 s^{-1}]	5.571×10^{-6}	8.322×10^{-6}[18,21]
D_{H_2}	[m^2 s^{-1}]	2.416×10^{-5}	3.765×10^{-5}[18,21]
D_{H_2O}	[m^2 s^{-1}]	1.407×10^{-5}	3.765×10^{-5}[18,21]

$$\vec{\nabla}\phi_{\text{ion}} = \frac{\vec{J}_{\text{ion}}}{\sigma_{\text{ion}}} \tag{14}$$

5. Boundary conditions

Unless explicitly indicated otherwise, internal-interface boundary conditions are set to ensure continuity between two contiguous domains. x and y directions refer to the directions in Fig. 1.

5.1. Gas channels

Boundary conditions for Eqs. (3)–(5) for both gas channels are:

- No-slip condition of the gas on the electrode/gas channel interface and gas channel/current collector walls.
- Gas velocity entering gas channel domain is known.
- Gas channel discharge pressure is the outlet operating pressure.
- Concentration entering the gas channel for every component, i, of the gas mixture is known.
- For channel outlet, only convection condition is considered.
- The remaining gas channel wall is isolated for mass transport.

5.2. Electrodes

Electrodes are in contact, on one side, with the gas and the current collector, and, on the other side, with the electrolyte, while the remaining surfaces are insulated.

The internal boundary conditions to solve mass transport equation are:

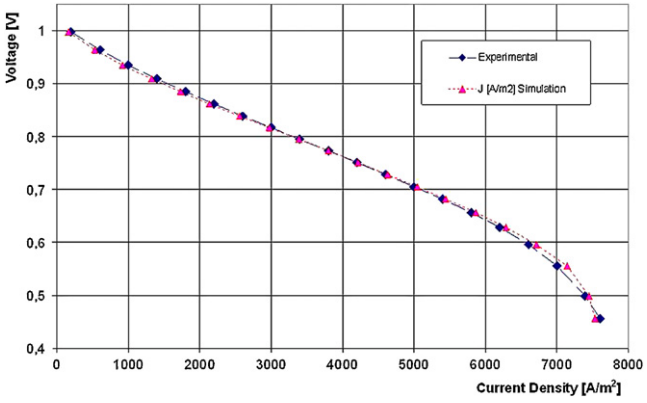

Fig. 6. Simulated and experimental polarization curves.

Table 3
Simulation vs. experimental parameters.

Voltage [V]	U_f^{lab} [%]	U_f^{sim}[%]	e_{Uf} [%]	J^{lab} [A m^{-2}]	J^{sim} [A m^{-2}]	e_J [%]
0.998	1.7	1.6	−5.88	200	190	−5.00
0.935	8.7	8.8	1.14	1000	1025	2.50
0.885	15.7	15.8	0.63	1800	1839	2.16
0.839	22.7	22.8	0.44	2600	2650	1.92
0.795	29.7	29.7	0	3400	3449	1.44
0.751	36.7	36.5	−0.54	4200	4244	1.04
0.705	45.5	43.3	−4.83	5000	5036	0.72
0.656	50.7	49.8	−1.77	5800	5788	−0.20
0.596	57.7	55.9	3.11	6600	6469	−1.60
0.498	64.7	64.1	−0.92	7400	7444	0.59
0.456	66.5	67.5	1.2	7600	7821	2.90

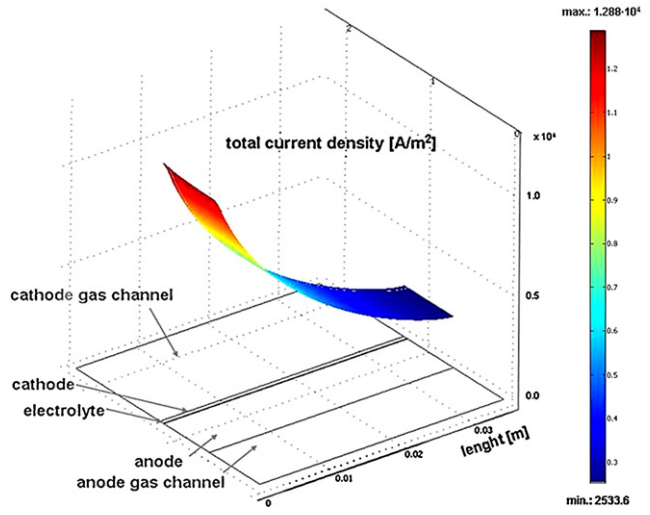

Fig. 7. Result for the current density in a 2D domain of a disk-shape anode supported SOFC ($V = 0.656$ V).

- at the electrode/electrolyte interface, gas species generated/consumed by electrochemical reactions (1) and (2), are related to the current density by the following equations:

$$\vec{n}\vec{N}_{H_2} = \frac{\vec{n}(\vec{J}_{el})}{2F} M_{H_2} \tag{15}$$

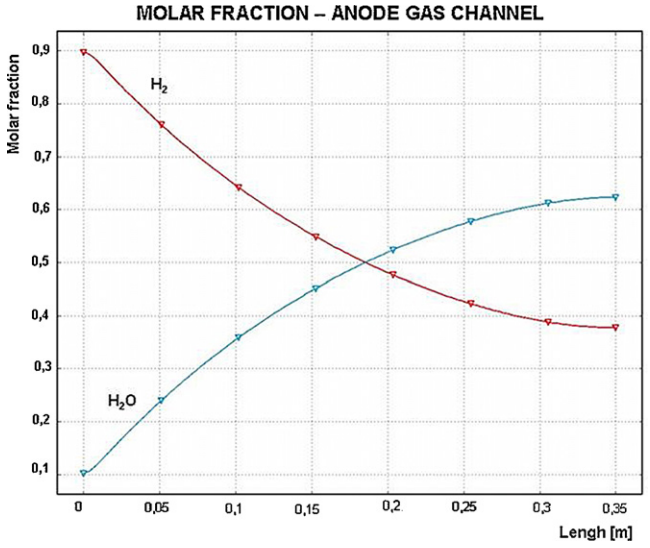

Fig. 8. Molar fraction of fuel components in the interface anode/gas channel along the cell ($V = 0.656$ V).

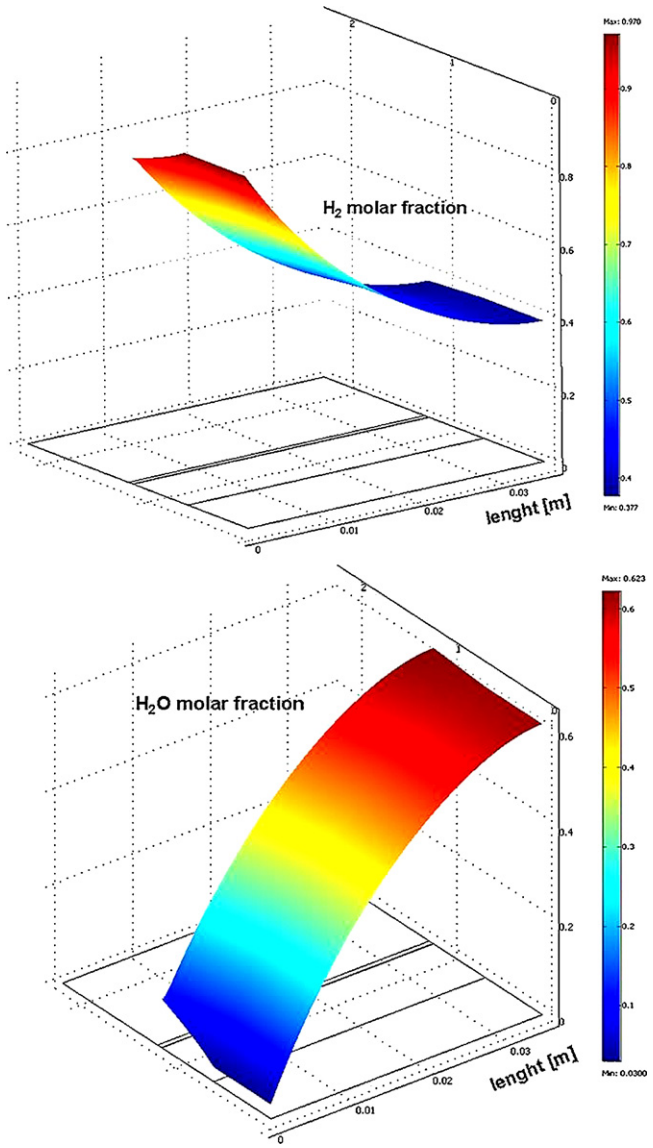

Fig. 9. Hydrogen and water mole fractions variation inside the anode ($V = 0.656$ V).

$$\vec{n}\vec{N}_{H_2O} = -\frac{\vec{n}(\vec{J}_{el})}{2F} M_{H_2O} \tag{16}$$

$$\vec{n} \cdot \vec{N}_{O_2} = -\frac{\vec{n} \cdot \left(\vec{J}_{el}\right)}{4F} M_{O_2} \tag{17}$$

The boundary conditions to solve the electrical problem within electrodes are:

- at electrodes/current collector interfaces, the boundary condition is given by the electrical potential

$$\begin{cases} \phi_{el,an} = 0 \\ \phi_{el,cat} = V_{cell} \end{cases} \tag{18}$$

Conditions (18) are applied under the assumption that the potential drop within the current collectors is negligible, which is justified by the high electrical conductivity of the current collectors, compared to those of the electrodes.

- at electrode/electrolyte interfaces, the boundary condition for the electric problem is given by the generated electrical current defined with the Butler–Volmer equation:

$$\vec{n}\vec{J} = J_o \left[\exp\left(\frac{n\beta F \eta_{act}}{R_g T} \right) - \exp\left(\frac{-n(1-\beta) F \eta_{act}}{R_g T} \right) \right] \quad (19)$$

where J_0 is the exchange current density and is computed for anode and cathode:

$$J_{o,an} = \gamma_{an} \frac{P_{H_2}}{P_{ref}} \left(\frac{P_{H_2O}}{P_{ref}} \right)^{-0.9} \exp\left(\frac{-E_{act,an}}{R_g T} \right) \quad (20)$$

$$J_{o,cat} = \gamma_{cat} \left(\frac{P_{O_2}}{P_{ref}} \right)^{0.25} \exp\left(\frac{-E_{act,cat}}{R_g T} \right) \quad (21)$$

η_{act} represents the activation loss, and is the difference between the ideal and real potential at the electrode/electrolyte interface:

$$\eta_{act} = \phi_{electrode} - \phi_{electrolyte} - V_{rev} \quad (22)$$

V_{rev} is computed with Nernst's equation, for anode and cathode [11]:

$$V_{rev,an} = -E_0 + \frac{R_g T}{nF} \ln\left(\frac{P_{H_2O}}{P_{H_2}} \right) \quad (23)$$

$$V_{rev,cat} = \frac{R_g T}{nF} \ln\left(\frac{P_{O_2}}{P_{ref}} \right)^{1/2} \quad (24)$$

Note that expressions (23) and (24) assume that most of the potential contribution is provided by the anode. This assumption is justified by the fact that the electrochemical reaction takes place at the anode side.

5.3. Electrolyte

There is no generation of ionic current inside the electrolyte domain but, as stated in assumption 1, in Section 4, at the electrolyte/electrode interface. Thus, an ionic current flows through the boundaries in contact with anode and cathode while the other boundaries of the electrolyte are insulated.

From the stoichiometry of reactions (1) and (2), two electrons pass through the external circuit when generating one oxygen ion. Thus, ionic current is a half of electronic current.

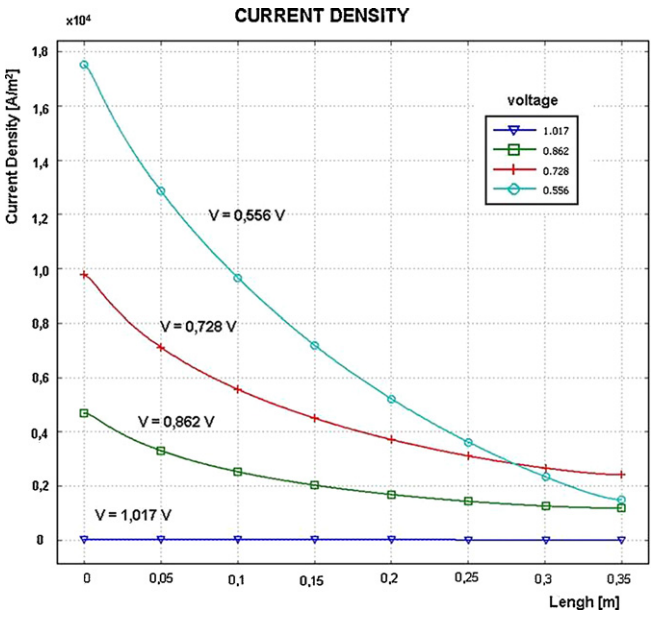

Fig. 10. Current density distribution for several voltages.

6. Model validation and results

The set of equations defined in Sections 4 and 5 are implemented and solved for steady-state conditions, using the commercial software for Finite Element Method resolution, COMSOL MULTIPHYSICS®.

Due to the symmetry of the cell, it is assumed that each radial section behaves in the same manner, thus a 2D representation of this section is used as the cell domain (Fig. 1). Operational parameters used for the simulation are those used during a set of experimental tests conducted at the Fuel Cell Group of the University of Perugia (Fig. 5). Operating conditions are: 1073 K, ambient pressure, humidified hydrogen for the anode feed (97% H_2 and 3% H_2O) and synthetic air as the oxidant flow (21% O_2 and 79% N_2 from industrial purity gas). Inlet gas flows are 24 Nl h^{-1} for the anode and 60 Nl h^{-1} for the cathode.

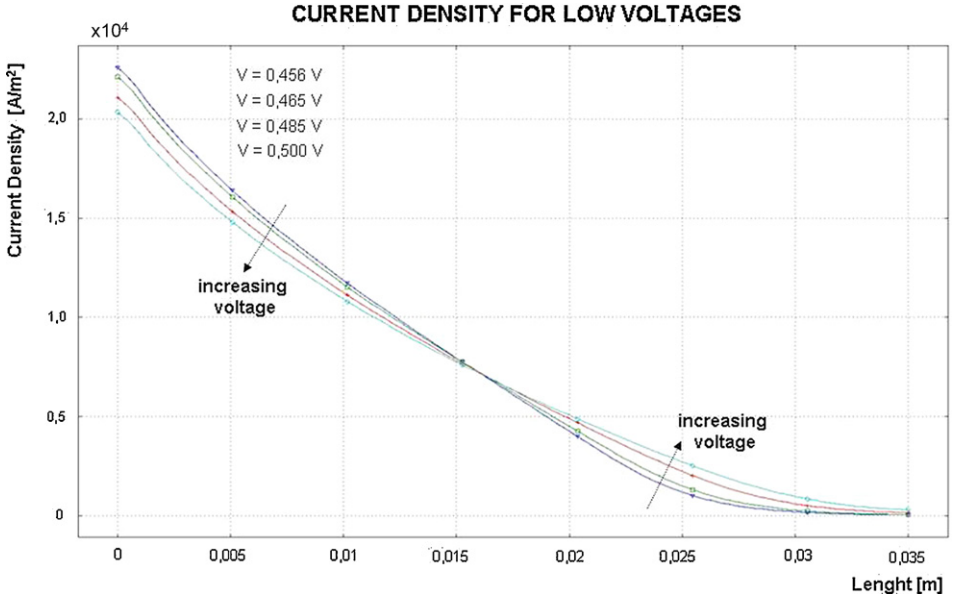

Fig. 11. Current density distribution for low voltages.

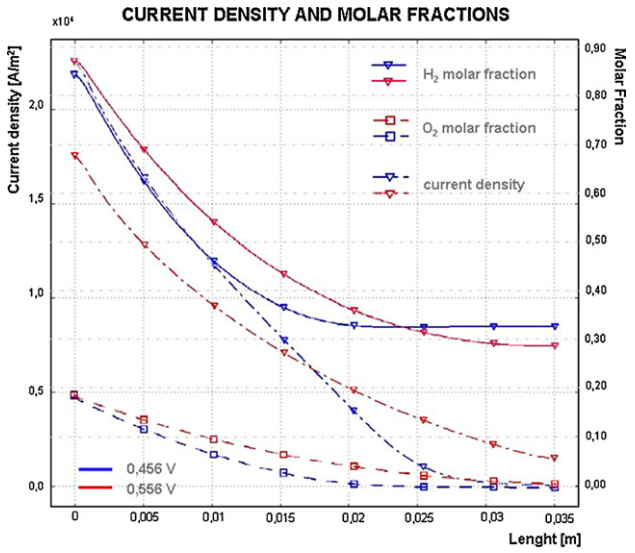

Fig. 12. Current density distribution vs. molar fraction of H_2, in anode side, and O_2, in cathode side.

In order to obtain the anodic and cathodic flow velocity in the considered 2D section, the following relation is applied:

$$U_{an,cat} = \frac{Q_{an,cat}}{2\pi r_{manif} h_{channel}} \quad (25)$$

$$Q_{an,cat} = N_i \left(\frac{T}{T_0}\right) \quad (26)$$

It should be noted that the choice of solving the problem in a 2D, rather than a 3D domain, leads to neglect the channel width variations along the radius, and, as the final consequence, to ignore the velocity reduction of the gas, as this proceeds along the gas channel. The present study is limited to obtain preliminary results on a 2D domain, and to verify the electrochemical performance predictions, and the convergence speed of the entire numerical simulation process. It must be stressed that the present preliminary results provide relevant useful indications on the cell operational conditions, with an acceptable accuracy of the results.

When comparing the calculated ideal open circuit voltage (OCV) to the experimental OCV, the introduction of an empirical factor, α_{OCV}, is required:

$$\alpha_{OCV} = \frac{OCV_{measured}}{OCV_{calculated}} \quad (27)$$

Several reasons explain the discrepancy between the calculated and measured OCV. Specifically, for the disk-shape SOFC, Momma et al. [23] measured a back-diffusion of cathodic gas into the outer region of the anode. However, the investigation of such phenomena is beyond the scope of the present paper.

Experimental works conducted at Forschungszentrum Jülich, Germany [24] and unpublished results obtained at Postech University, in South Korea [25], show that when assembled and operated in an entire fuel cell, single components show different electrical proprieties, compared to those of single samples not embedded in a fuel cell. Both [24,25] noticed a conductivity reduction, not directly correlated to the anode and cathode materials themselves, but to the contact between them and the electrolyte. As a consequence of these effects, data available in the literature for SOFC components conductivity are not directly applicable for fuel cell simulations. For this reason, these values have been extrapolated from the comparison with the experimental data.

By comparing the results of the model with the experimental data, a calibration of the parameters is obtained. The calibrated parameters and the corresponding values found in the literature

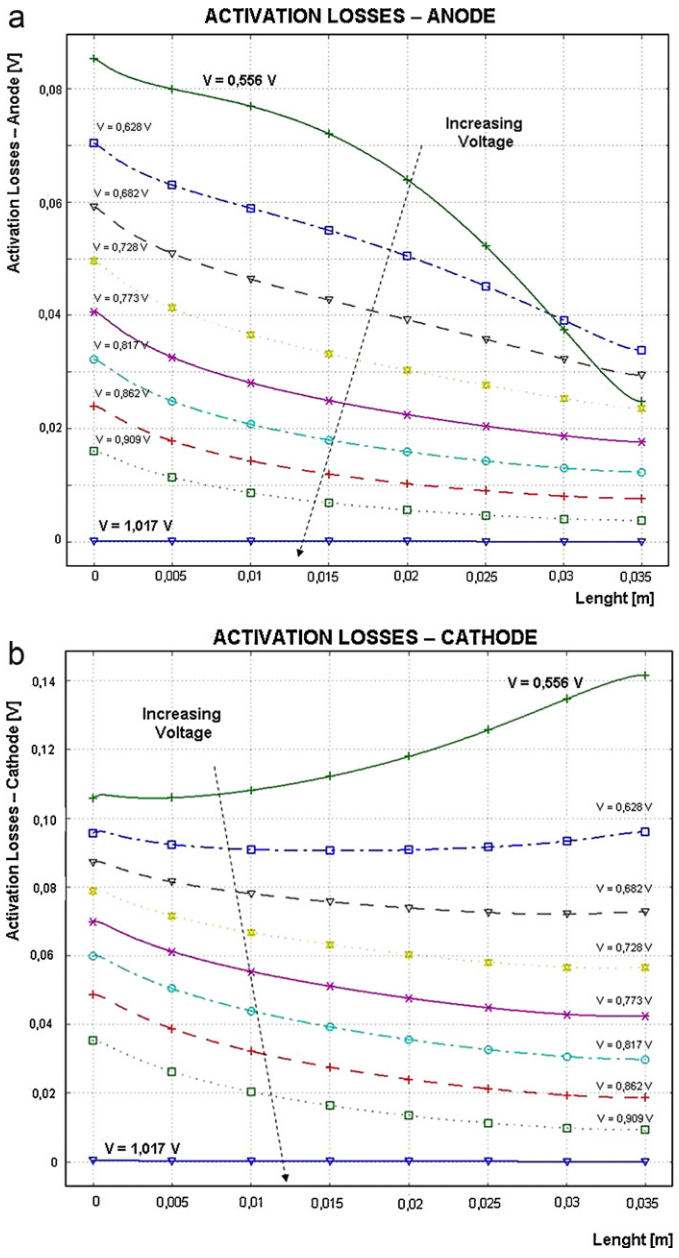

Fig. 13. (a) Activation losses at anode interface and (b) activation losses at cathode interface.

are compared in Table 2. Fig. 6 illustrates that the experimental and calculated polarization curves are mostly coincident but in the initial part, where losses related to energy of activation are dominant. Table 3 presents the values of voltage versus current density and coefficient of utilization of the fuel (simulated and experimental) and the corresponding percentual error. The error never exceeds 5% for the current density, and reaches 5.8% for the fuel utilization.

Fig. 7 shows the distribution of the current density in the entire domain when the cell voltage is 0.656 V. The current density, as expected, diminishes while hydrogen is consumed along the cell.

Fig. 8 presents hydrogen and water mole fractions profiles along the cell length in the gas channel (interface gas channel/electrode), when the cell voltage is 0.656 V. Fig. 9 shows H_2 and H_2O mole fraction variation within the whole anode domain, and, together with Fig. 8 illustrate the impact of the occurrence of hydrogen oxidation.

Results shown in Figs. 7–9 are referred to a specific electric load demand, characterized by a cell voltage of 0.656 V. This value can be considered as a typical cell voltage for SOFC.

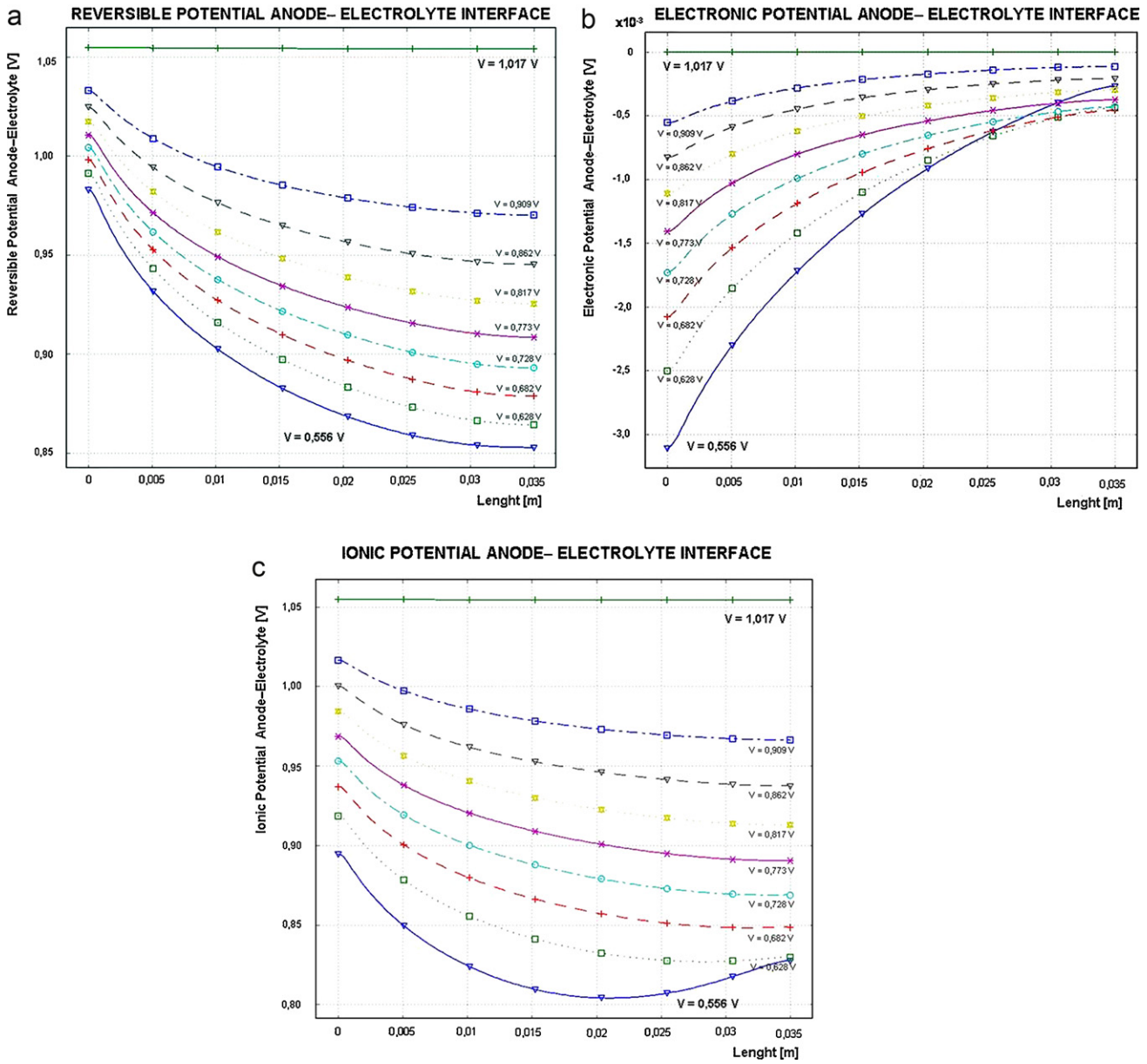

Fig. 14. (a) Reversible voltage at anode–electrolyte interface, (b) electronic potential distribution at anode–electrolyte interface, and (c) ionic potential distribution at anode–electrolyte interface.

However, it is important to investigate the internal condition of a single cell for other load requirements.

As illustrated in Fig. 1, since the current collection is performed via a metallic mesh located on the entire surface of the electrode in the gas channel, the current path is perpendicular to the cell plane, i.e. the current density is uniform along the cell thickness, thus one dimensional graph can fairly describe the current density distribution inside the cell.

The current density profile, for several applied voltages, is shown in Fig. 10. As the applied voltage decreases, the total current provided by the cell increases. Since the inlet fuel and oxidant flow rates are constant, the fuel and oxidant utilizations increase as the applied voltage decreases. For high fuel or oxidant utilizations, a gas starvation takes place locally, in some regions of the two electrodes, thus generating a strong current density reduction. As visible in Fig. 10, for a voltage as low as 0.556 V, the current density reduction along the cell is very pronounced.

As shown in Fig. 11, for voltages below 0.5 V, the outer part of the cell is not properly exploited, i.e. the current density becomes close to zero (75 times smaller than maximum local value of current density) at the exit of the cell. Eqs. (15)–(17) show that current density is directly related to hydrogen, water and oxygen consumption/production, thus gas starvation and the drop of current density are strictly connected. Such operational condition should be avoided, especially for long term operation, because it leads to severe materials degradation issues [26–28].

As shown in Fig. 12, in the present case, the current density reduction is due to oxygen starvation at the cathode.

A better distribution of the current density and, consequently, a reduction of local gas starvation could be achieved via an increasing porosity of the electrodes from the inlet to the outlet. With the present fuel cell technology, however, it is preferable to operate the fuel cell at reduced fuel and oxygen utilization. It should be noted that when a stack is operated, the stack temperature is regulated

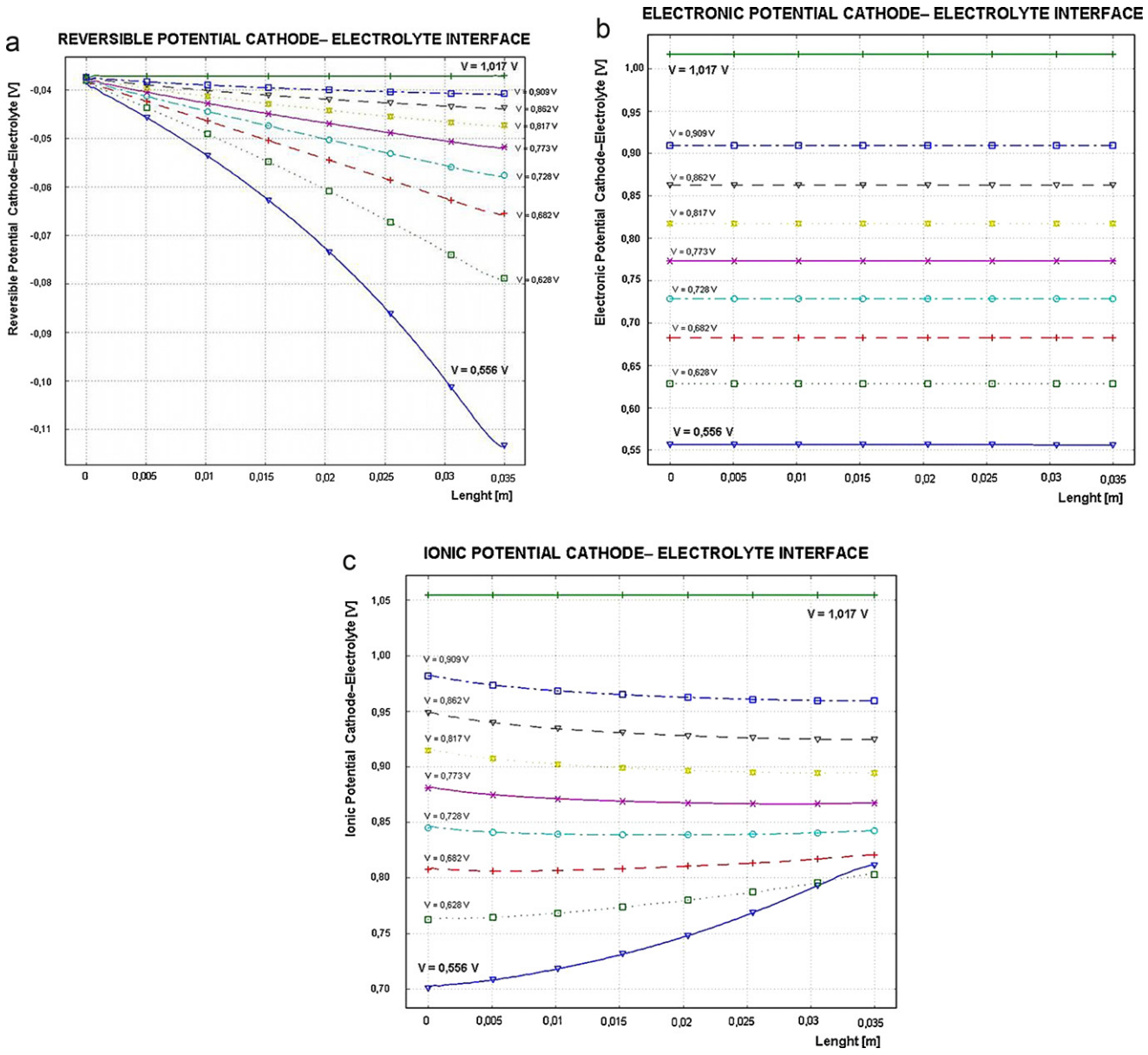

Fig. 15. (a) Reversible voltage at cathode–electrolyte interface, (b) electronic potential distribution at cathode–electrolyte interface and (c) ionic potential distribution at cathode–electrolyte interface.

by the air flow rate. The energy balance imposes an air flow rate that is generally within a range of 3–7 times the stoichiometric value [29,30]. For this reason, oxygen local starvation is not an issue for SOFC when operated in a stack. On the other hand, in order to achieve high conversion efficiency, fuel utilization needs to be kept as high as possible. An engineering solution is to recycle the anode outlet to the inlet, so that the overall fuel utilization of the system is kept high, even if the fuel cell operates with reduced fuel utilization [31–33].

Fig. 13a and b illustrates the activation losses along the cell length. According to assumption 1, Section 4, the electrochemical reactions take place at the electrode/electrolyte interface; therefore activation losses occur in these surfaces (reduced to lines in the 2D schematization).

Activation losses depend on gas concentration and current density, as shown in relations (19)–(24). The high oxidant utilization corresponding to $V = 0.556\,V$ leads to an extremely low oxygen concentration and, as a consequence, to different distributions of activation losses for the anode and for the cathode.

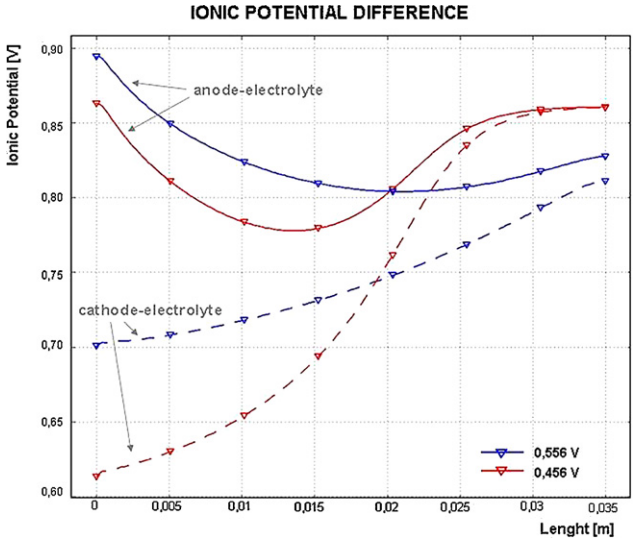

Fig. 16. Trend of ionic potentials at anode and cathode interfaces for low voltages.

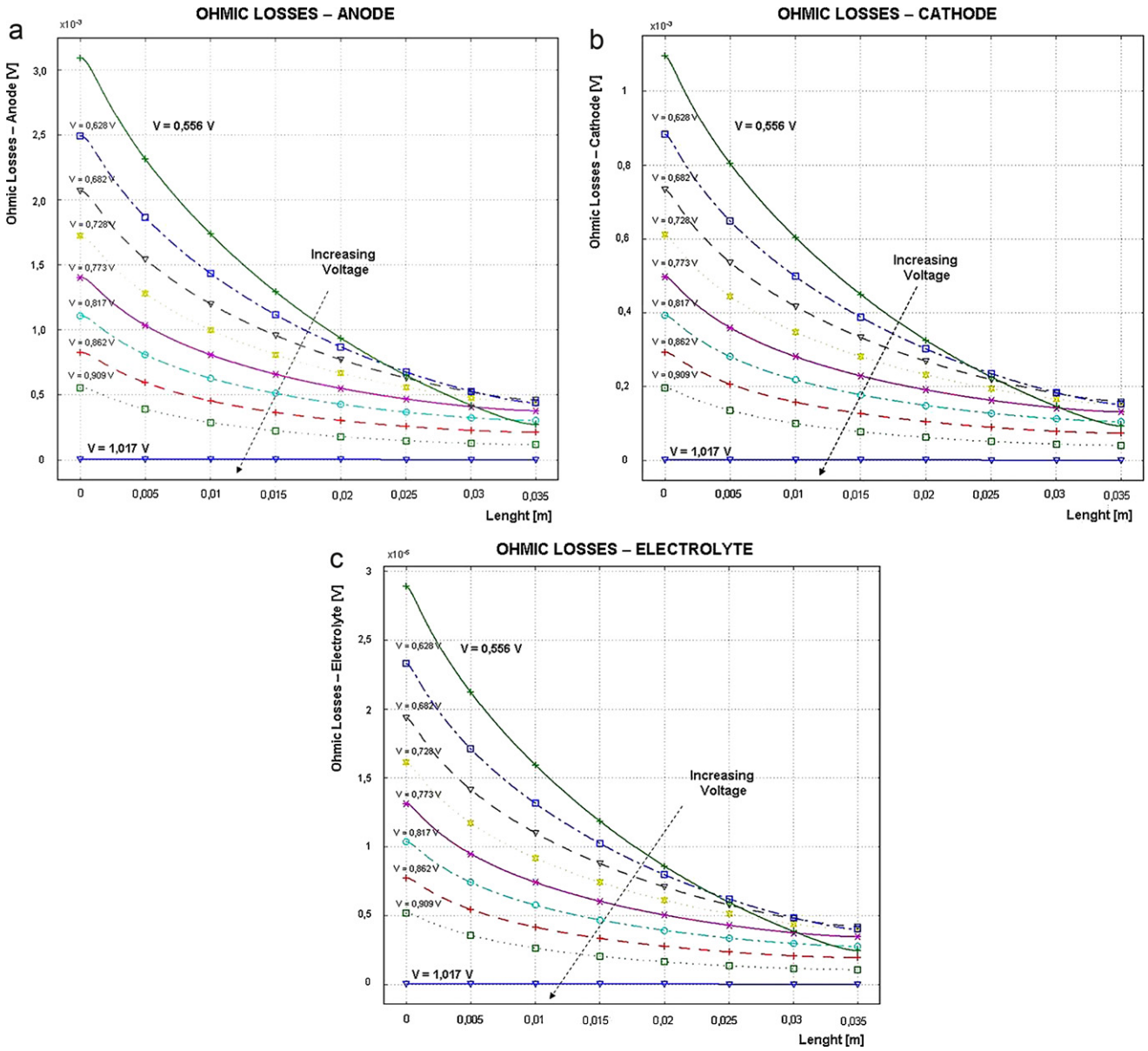

Fig. 17. (a) Ohmic losses in anode domain, (b) Ohmic losses in cathode domain, and (c) Ohmic losses in electrolyte domain.

Fig. 14a–c presents the variation of the terms used for the calculation of the anode activation losses in order to identify the cause of this behaviour. Considering the orders of magnitude, it may be stated that the anode activation losses are controlled by the difference between reversible potential and ionic potential at the electrolyte–anode interface (electronic potential is negligible), Eqs. (22) and (23).

Fig. 15a–c shows the terms involved in calculation of the cathode activation losses, Eqs. (22) and (24). In this case, the electronic potential is not negligible and its evolution along the length of the cell is mostly constant, thus the distribution of the cathodic activation losses is mainly controlled by the ionic and reversible potentials.

The effect of oxygen starvation for $V = 0.556$ V or lower voltages is directly connected to the difference of ionic potential between anode–electrolyte and cathode–electrolyte interfaces. Fig. 16 shows the trend of these two potentials at both interfaces for low voltages (0.556 V and 0.456 V) due to progressive starvation of oxygen near the outlet. In this region, it is clearly visible that the difference of potentials for 0.456 V becomes zero, leading to zero current density.

If a PEN lumped structure is assumed for modelling the fuel cell [4–9], the mass transport inside the porous media is not directly modelled. However, the gas concentration in the bulk is different from that at the reaction zone, due to mass transport phenomena, thus the voltage calculated with gas concentration in the bulk is higher than that calculated at the reaction zone (TPB). As a consequence, numerical models assuming a PEN structure, usually introduce so-called concentration losses, which quantify the voltage reduction, due to the mass transport phenomena within the electrodes. This loss is deduced, together with the activation and the ohmic losses, to OCV, in order to calculate the cell voltage [4–9].

Although with the modelling approach adopted for the present study, it is not necessary to introduce such a computation for evaluating the cell voltage, it is useful to evaluate, as a post processing operation, the effect of the mass transport.

This is done by calculating the difference between Nernst voltage at the bulk and at the reaction zone:

$$\eta_{\mathrm{conc,an}} = -\frac{R_g T}{nF} \ln\left(\frac{P'_{\mathrm{H_2}}}{P_{\mathrm{H_2,bulk}}} \frac{P_{\mathrm{H_2O,bulk}}}{P'_{\mathrm{H_2O}}}\right) \quad (28)$$

$$\eta_{\mathrm{conc,cat}} = -\frac{R_g T}{nF} \ln\left(\frac{P'_{\mathrm{O_2}}}{P_{\mathrm{O_2,bulk}}}\right)^{1/2} \quad (29)$$

As expected, since the anode is much thicker than the cathode, the anode concentration loss is much higher than the cathodic one. This trend, however, changes for very high current densities and fuel utilizations, i.e. for a low cell voltage.

Finally Fig. 17a–c represents the ohmic losses at the anode, cathode and electrolyte, respectively. Since the electrical and ionic conductivity are assumed homogenous within each domain, the trend in ohmic losses is the same of the current density.

7. Conclusions

Numerical simulations of SOFC are still in an early stage of development because of the relative novel interest in SOFC and the complexity of the process coupling.

Most of the current mathematical models are not capable to simulate the entire domain, because the assumed lumped PEN structure. In addition, they are restricted to just one specific geometry.

The detailed model presented in this paper is based on partial differential equations and can be applied to different geometries and cell materials. In the present study, the model was implemented and validated on a disk-shape planar single cell. Experimental data for validation are obtained at the FC lab of the University of Perugia. Numerical and experimental results show a good agreement, with an error below 5% for the current density, and 6% for the fuel utilization. The results obtained allow visualization of the evolution of the most important physical variables in the entire fuel cell domain, thus identifying limiting phenomena, such as local gas starvation at high fuel and oxidant utilization, and the contribution of mass transport, ohmic losses and activation losses to the voltage reduction.

8. Further development

Three main limitations of the model are amenable to further developments to create a more robust and efficient tool for designing SOFC and predicting the behaviour.

(1) This model refers to humidified hydrogen as fuel. To simulate the behaviour of a fuel cell operating on other gases, a mathematical model capable of describing internal reforming and equilibrium (water-shift) reactions within the anode side must be defined.
(2) In this paper, energy balance is not taken into consideration because the fuel cell from which experimental data are taken is operated in an isothermal atmosphere, controlled by an electric furnace. An extension of the model will be to implement energy equations and to compare the resulting temperature distribution to that of a single cell embedded in a stack.
(3) The implementation of the model at non-steady-state-conditions, and in a 3D domain.

References

[1] R. Bove, Technical and environmental evaluation of high temperature fuel cell through numerical simulations and in field tests, PhD Thesis. University of Perugia, Italy, 2004.
[2] P. Lunghi, U. Ubertini, Proceedings of the 7th International Symposium on Solid Oxide Fuel Cells, Tsukuba, Ibaraki, Japan, 2001, pp. 254–264.
[3] P. Lisbona, A. Corradetti, R. Bove, P. Lunghi, Electrochim. Acta 53 (2007) 1920–1930.
[4] A. Bjaradwaj, D.H. Archer, E.S. Rubin, J. Fuel Cell Sci. Technol. 2 (2005) 52–59.
[5] A. Bjaradwaj, D.H. Archer, E.S. Rubin, J. Fuel Cell Sci. Technol. 2 (2005) 38–44.
[6] E. Achenbach, J. Power Sources 49 (1994) 333–348.
[7] H. Yakabe, M. Hishinuma, M. Uratani, T. Matsuzaki, I. Yasuda, J. Power Sources 86 (2000) 423–431.
[8] P. Aguiar, D. Chadwick, L. Kershenbaum, Chem. Eng. Sci. 57 (2002) 1665–1677.
[9] P. Costamagna, A. Selimovic, M. Del Borghi, G. Agnew, Chem. Eng. J. 102 (2004) 61–69.
[10] R. Bove, P. Lunghi, N.M. Sammes, Int. J. Hydrogen Energy 30 (2005) 189–200.
[11] J.R. Ferguson, J.M. Fiard, R. Herbin, J. Power Sources 58 (1996) 109–122.
[12] A.K.M. Podias, G. Tsotridis, in: D. Tsahalis (Ed.), Proceedings of the 1st International Conference "From Scientific Computing to Computational Engineering", vol. 2, University of Patras Press, 2004, pp. 765–775.
[13] J.J. Hwang, C.K. Chen, D.Y. Lai, J. Power Sources 143 (1–2) (2005) 75–83.
[14] U. Pasaoguillari, C.-Y. Wang, Proceedings of the Eighth International Symposium on Solid Oxide Fuel Cells (SOFC VIII), vol. 2, Paris, France, April 27–May, 2003, p. 1403.
[15] R. Bove, N.M. Sammes, Proceedings of the Ninth International Symposium on Solid Oxide Fuel Cells (SOFC IX), May 15–20, Quebec City, Canada, 2005.
[16] R. Bove, S. Ubertini, Modeling Solid Oxide Fuel Cell Operation: Models. Procedures and Techniques, Springer, 2008, Chapter 3.
[17] A.C. Burt, I.B. Celik, R.S. Gemmen, A.V. Smirnov, J. Power Sources 126 (2004) 76–87.
[18] Z. Shan, R.T. Jacobsen, S.G. Penoncello, Int. J. Thermophys. 22 (2001) 73–87.
[19] B. Todd, J.B. Young, J. Power Sources 110 (2002) 186–200.
[20] G. Karaiskakis, D. Gavril, J. Chromatogr. A (2004) 1037.
[21] S.H. Chan, K.A. Khor, Z.T. Xia, J. Power Sources 93 (2001) 130–140.
[22] P. Aguiar, C.S. Adjiman, N.P. Brandon, J. Power Sources 138 (2004) 120–136.
[23] A. Momma, Y. Kaga, K. Takano, K. Nozaki, A. Negishi, K. Kato, T. Kato, T. Inagaki, H. Yoshida, K. Hoshino, M. Yamada, T. Akbay, J. Akikusa, J. Power Sources 145 (2) (2005) 169–177.
[24] E. Wanzenberg, F. Tietz, D. Kek, P. Panjan, D. Stöver, Solid State Ionics 164 (2003) 121–129.
[25] Personal communication with Prof. G.M. Choi, director of the Fuel Cell Center of Pohang University of Science and Technology, South Korea, November 2005.
[26] D. Larrain, Solid oxide fuel cell stack simulation and optimization, including experimental validation and transient behaviour. PhD Thesis No 3275, École Polytechnique Fédérale De Lausanne, 2005.
[27] G. Robert, A. Kaiser, E. Batawi, in: M. Mogensen (Ed.), Proc. of the 6th European SOFC Forum, 2004, pp. 193–200.
[28] D. Waldbillig, A. Wood, D.G. Ivey, Solid State Ionics 176 (9–10) (2006) 847–859.
[29] P. Lunghi, R. Bove, A. Corradetti, P. Lisbona, Proceedings of the 7th European SOFC Forum, July 3–7, Lucerne, Switzerland, 2006.
[30] J. Van Herle, F. Maréchal, S. Leuenberger, Y. Membrez, O. Bucheli, D. Favrat, J. Power Sources 131 (2004) 127–141.
[31] S. Campanari, J. Power Sources 92 (1–2) (2001) 26–34.
[32] T. Kivisaari, P. Björnbom, C. Sylwan, B. Jacquinot, D. Jansen, A. de Groot, Chem. Eng. J. 100 (2004) 167–180.
[33] A. Heinzel, J. Roes, H. Brandt, J. Power Sources l145 (2005) 312–318.